Spectroscopy and optical characterization of thulium doped TZN glasses

Spectroscopy and optical characterization of thulium doped TZN glasses

H. Gebavi [1,*], D. Milanese[1], R. Balda[2], S. Chaussedent[3], M. Ferrari[4], J. Fernandez[2], M. Ferraris[1]

[1]Dipartimento di Scienza dei Materiali ed Ingegneria Chimica, Politecnico di Torino, Corso Duca degli Abruzzi 24, 10129 Torino, Italy, email: gebavi@yahoo.com

[2]Departamento de Fisica Aplicada I, Escuela Superior de Ingenieros, Alda. Urquijo s/n 48013 Bilbao, Spain and Center of Materials Physics CSIC-UPV/EHU and Donostia International Physics Center, Apartado 1072, 20080 San Sebastian, Spain

[3]Laboratoire POMA-FRE CNRS 2988, Universite d'Angers, 2 bd. Lavoisier, 49045 Angers, France

[4]CNR-IFN, CSMFO Lab., via alla Cascata 56/C, 38050 Povo-Trento, Italy

Abstract

This paper reports spectroscopic properties of the $^3H_4$ and $^3F_4$ Tm^{3+} levels in TZN glass host with a concentration range from 0.82 to 22 10^{20} cm^{-3}. Precise refractive index measurements are performed on five different wavelengths by the prism coupling method. Judd – Ofelt intensity parameters have been determined in order to obtain transition rate, branching ratio, and radiative lifetime. Spectroscopy measurements showed the most promising concentration for 1.8 μm short cavity laser emission at 6.84 10^{20} cm^{-3} Tm^{3+} with a 24% quantum efficiency and upper limit concentration of 11 10^{20} cm^{-3} Tm^{3+}. Energy transfer microparameters and critical ion distance are determined for both emission levels in the framework of diffusion – limited regime and dipole – dipole interaction.

Keywords: tellurite glass, thulium, Judd-Ofelt, refractive index, energy transfer

PACS: 42.70.Hj; 78.40.-q; 78.55.-m; 78.55.Qr.

1. Introduction

Huge scientific effort was devoted in investigation materials and devices for emission in the infrared wavelength region where optical telecommunications play their main role, in the so called S–band from 1460 to 1530 nm, C–band from 1530 to 1565 nm and L–band from 1565 to 1625 nm. On the other hand, infrared (IR) domain at wavelengths around 2 μm includes different properties and offers a number of applications. First of all, there is an atmospheric transparency window that allows remote sensing in free space. Detection of

water vapor is also possible in such range of wavelengths, thanks to strong vibrational absorption lines [1].

Thulium (Tm^{3+}) is a good choice for IR domain applications because of its absorption at 790 nm which is available using commercial diodes, and its interesting emission at ~ 1.8 μm for a number of sensing and medical applications [2]. In addition, the phonon assisted energy transfer process called "cross relaxation"(CR: $^3H_4$, $^3H_6 \rightarrow {}^3F_4$, $^3F_4$) allows obtaining two ions in upper laser level for each pumping photon, which enhances the 1.8 μm emission and is one of the main reasons for utilizing thulium as an active ion for IR applications. An important feature of Tm^{3+} as emitter in a host glass is the possibility of continuous tuning in the 1.8 - 2 μm region depending on the host matrix, thanks to its wide emission peak. Tunability of Tm is also demonstrated in the 2.2 – 2.46 μm region in Tm:YLF host (crystal host) for small dopant concentrations [3].

Another interesting emission in the eye–safe region and telecommunication S-band is at 1.47 μm which occurs for $^3H_4 \rightarrow {}^3F_4$ transition. However, inverted population for such lasing transition is more difficult to obtain without depopulating the lower energy level since the lifetime of $^3H_4$ level is shorter than the one of $^3F_4$ which creates the so called 'bottleneck' effect.

The aim of this study is a detailed glass examination in order to improve fiber lasing emission and develop short cavity fiber laser with lasing emission in the infrared region. Advantages of a short laser cavity lies in a background loss reduction which occurs due to scattering or contaminants absorption and so can yield the same gain in a shorter device [4] and narrow emission linewidth. Such objective requires highly doped active ion concentration which carries a potential risk of clustering and increasing of excited state absorption effect (ESA) or reverse cross-relaxation. Fiber lasers have potential for narrow linewidth (few kHz) applications compared with for example semiconductor lasers (~ MHz). [4]. Narrow linewidth

is specially related to single frequency laser which operates in a single resonator mode emitting quasi monochromatic radiation with very small linewidth and phase noise which guarantees spectral purity. The origin of the phase noise is spontaneous emission of the gain medium related with optical and technical noise influence. The short cavity should give contribution to stabile long–term, single mode operation avoiding hopping mode [5]. On the other hand, too narrow linewidth can create problems due to Brillouin scattering which can be partially reduced by resonator length decrease [5].

As the host matrix tellurite glass is used because of its unique properties whilst the IR emission is ensured with thulium ions. In a previous work [6], some of the authors reported a characterization of some structural and optical properties of Tm^{3+} ions in $75TeO_2$-20ZnO-$5Na_2O$ tellurite glass. In this work, we report together with Judd–Ofelt analysis to calculate transition rates, radiative lifetimes, and branching ratios the study of the effect of concentration on the $^3H_4 \rightarrow {}^3F_4$ and $^3F_4 \rightarrow {}^3H_6$ emissions of Tm^{3+}. Wide concentration range strongly changes the nature of the ion-ion interaction which is characterized by quenching parameters. The analysis of the fluorescence decays from the $^3H_4$ level indicates the presence of a dipole-dipole quenching process assisted by energy migration. Energy transfer microparameters and critical ion distance are determined for both emission levels $^3H_4$ and $^3F_4$, in the framework of diffusion – limited regime and dipole – dipole interaction.

2. Experimental techniques

2.1. Glass fabrication

Glasses were prepared by melt quenching from mix powder batches, inside a glove box in a dry atmosphere with water content of about 7 ppm. The chemicals employed (together with their purity) were the following: TeO_2 (99+%), ZnO (99.99%), Na_2CO_3

(99.995%), Tm_2O_3 (99.99%). Relative molar ratio of the host glass constituent oxides was kept the same for all samples, regardless of Tm doping. The fabricated samples were based on the host glass composition $75TeO_2$:20ZnO:$5Na_2O$ and doped with increasing amounts of Tm^{3+}. Nine different samples were prepared with the following Tm^{3+} mol% content with respect to the glass constituent oxides: 0.36, 1, 2.1, 3, 4, 5, 6, 7 and 10. Glass melting was carried out in Pt crucibles at around 900 °C for 2-3 h, followed by pouring on a preheated brass plate at 300 °C and annealing followed. The whole process required around 20 h of operation.

2.2 *Glass characterization: optical properties*

Glasses were cut into 1-2 mm thick slices and polished to an optical quality. UV-VIS spectroscopy in transmission was carried out with a Varian Cary 500 spectrometer in order to assess the absorption spectra of the rare earth doped glasses.

Refractive index was measured for all samples at five different wavelengths (533, 825, 1061, 1312 and 1533 nm) by the prism coupling technique (Metricon, model 2010). The resolution of the instrument was of ± 0.0001. Five scans were used for each measurement. Standard deviation in refractive index at different points of the same sample was around ±0.0003.

The steady-state emission measurements were made with a Ti-sapphire ring laser (0.4 cm^{-1} linewidth) at 793 nm of excitation wavelength. The fluorescence was analyzed with a 0.25 monochromator, and the signal was detected by a PbS detector and finally amplified by a standard lock-in technique. Lifetime measurements were obtained by exciting the samples with a Ti-sapphire laser pumped by a pulsed frequency doubled Nd:YAG laser (9 ns pulse width), and detecting the emission with a Hamamatsu R5509-72 photomultiplier. Since the R5509-72 PMT showed weak response at ~1800nm, the decay curves from $^3F_4$ level (Tm^{3+})

were performed by collecting the luminescence at the emission wavelength of 1680 nm. Data were processed by a Tektronix oscilloscope. All measurements were performed at room temperature.

3. Experimental results

3.1. Glass table and refractive index measurements

Table 1 shows the samples examined in this study together with their dopant concentration and refractive index values at 633, 825, 1061, 1312 and 1533 nm respectively. The refractive index decreases with increasing Tm^{3+} concentration and increasing wavelength [6]. Values of the refractive index of the sample T5 are used for obtaining Cauchy fitting parameters to be used in the Judd – Ofelt theory (3.2).

3.2 Judd-Ofelt theory results

The VIS-NIR absorption measurement was obtained in the 300-2100 nm range on the sample doped with 11.3 10^{20} cm^{-3} Tm^{3+}, T5 (58151 ppm of Tm^{3+}). Absorption transitions originating in the ground state are assigned as $^1G_4$, $^3F_{2,3}$, $^3H_4$, $^3H_5$ and $^3F_4$ (Fig.1.).

Judd–Ofelt (J-O) theory is used to calculate transition probabilities between different manifolds, radiative lifetimes and emission branching ratios as found in the literature [7, 8]. Obtained values of J – O parameters by using five main absorption bands are summarized in Table 2 together with the literature overview.

The absorption bands of Tm^{3+} are all dominated by electric dipole transitions except the transition $^3H_6 \rightarrow {}^3H_5$, which contains electric-dipole and magnetic-dipole contributions which can be calculated as shown in the literature [8]. The largest error in a J-O calculation is

the assumption that all Stark levels of a given multiplet are equally populated. An overview of radiative rate, lifetime, and branching ratio of the main transitions is given in Table 3.

In section 3.4 is introduced the experimental value obtained on a low doped sample and considered as radiative lifetime. Comparison of lifetime results given by the J-O theory with experimental values and the results from other authors is presented in Table 4.

All reported data indicate the radiative value of $^3H_4$ level as ~0.35 ms whilst a significant discrepancy for $^3F_4$ level between J-O theory and the experimental values is observed.

3.3 Emission spectra

Emission spectra of $^3H_4 \rightarrow {}^3F_4$ and $^3F_4 \rightarrow {}^3H_6$ transitions correspond to 1475 and 1847 nm emissions, respectively. Fig 2 shows the spectra of all prepared samples: they are normalized on the area under the $^3H_4$ level emission band. Some of the emissions (sample T7 and T4) from $^3F_4$ level are shifted towards longer wavelengths which is due to measurements on thicker samples and therefore affected by reabsorption effects.

Fig. 3a presents the ratio between the areas under $^3H_4$ and $^3F_4$ emission bands. Increase of $^3F_4$ emission with dopant increase is likely due to CR between $^3H_4 \rightarrow {}^3F_4$ and $^3F_4 \rightarrow {}^3H_6$ transitions. Saturation occurs for Tm^{3+} concentrations higher than 6 mol% of Tm^{3+}. In that case $^3H_4$ level is totally depleted by CR to $^3F_4$ level and no further increase in the 1847 nm emission is possible.

Fig. 3b presents the ratio between the same two emission peaks normalized to the number of ions. This ratio could give an insight about the concentration dependence of the efficiency of the cross-relaxation process. Two regions can be observed: the first one, when the emission at 1847 nm increases, up to 3 mol%, and the second one for higher concentrations when it decreases. The peak value is for the sample doped with 3 mol% of

Tm^{3+}. CR process is beneficial up to 3 mol% of Tm^{3+} considering the amount of dopant Tm^{3+} ions. Above this concentration, quenching of $^3F_4$ level begins.

Emission cross section can be calculated by using the expression [9]: $\sigma_{em.} = \frac{\lambda_p^4 \beta}{8\pi n^2 c \tau_0 \Delta\lambda_{eff}}$, where λ_p is the peak fluorescence wavelength, β is branching ratio, n is refractive index, c is light velocity, τ_0 is radiative lifetime and $\Delta\lambda_{eff.}$ is the effective linewidth.

The effective linewidth of the transition has been calculated by using the relation $\Delta\lambda_{eff} = \int \frac{I(\lambda)}{I_{max}} d\lambda$. The emission cross section obtained values for level $^3H_4$ are in the range 2.6-2.8 10^{-25} m^2 whilst for level $^3F_4$ emission values of the T0.36 sample is 5.4 10^{-25} m^2. This value is in agreement with those reported in the literature for tellurite glasses [8, 9] and higher than those reported in fluoride and oxyfluoride glasses [10].

Fluorescence waveforms were measured at 1475 nm ($^3H_4$ level) and 1680 nm ($^3F_4$ level) by pumping with 793 nm excitation wavelength at room temperature. Further experimental results and discussion will be separately presented for both emissions.

3.4. Concentration quenching of the $^3H_4$ emission

The decay curves for the $^3H_4$ level at 1475 nm were found to be non-exponential for all dopant concentrations except for the 0.36 mol% Tm^{3+} doped sample (T0.36) which shows an exponential decay i.e. linear curve in semilogarithmic scale, as reported in Fig. 4.

Average lifetime values for the non-exponential decays are calculated by utilizing the expression [13]: $\langle\tau\rangle = \frac{1}{I(t=0)} \cdot \int I(t)dt$. Calculated lifetime values from this expression are given in Table 5. The lifetime value of the lowest doped sample T0.36 is taken as the radiative lifetime in further assumptions.

Photoluminescence quantum efficiency (η) is expressed as a ratio between number of emitted and incident excitation photons. By the formula, η can be described either as a ratio between radiative and total decay or as the ratio between measured and radiative lifetime $\eta = \tau_m/\tau_0$ [14]. Quantum efficiencies of all glass samples are reported in Table 5.

The reduction of the lifetime and quantum efficiency of the 1475 nm emission as concentration increases, together with the change from exponential to nonexponential decays have been previously observed in Tm-doped glasses and attributed to cross-relaxation processes such as $^3H_4$, $^3H_6 \rightarrow {}^3F_4$, $^3F_4$. In this process part of the energy of an ion in level $^3H_4$ is transferred to another ion in the ground state with both ions ending up in level $^3F_4$.

Energy transfer (ET) occurs when more than one optically active center are present inside the critical domain. Its value depends on sensitizer emission and activator absorption spectra overlapping, mutual ion distance, quantum transition efficiency, relative orientation of sensitizer and acceptor transition dipoles [15]. ET processes can be considered as radiative or non–radiative. In the case of radiative processes characterized by photon transfer, there is no coupling between active ions, and their emission probability will remain the same. However, non–radiative energy migration can be described by Coulomb interaction via electromagnetic field or by quantum mechanic and virtual photon exchange. The latter can be transferred to a classical mechanic frame by a dipole oscillator interaction assumption. Dipole – dipole (dd) and multipole interaction theory is described in the work by Dexter and Förster [16].

Non-radiative energy transfer processes such as cross-relaxation are generally described in terms of three limiting cases: a) one step process involving direct energy transfer, b) diffusion - limited relaxation, and c) fast diffusion [17]. In the case of very fast diffusion, the decay of the donor fluorescence is purely exponential.

Decay curve of sample T0.36 (Fig. 4) shows a clear exponential decay and can be described by direct energy transfer model. However, for the higher dopant concentration it was not the case. Difference between diffusion limited process and fast diffusion can be determined by the concentration dependence of the quenching rate R_Q given by:

$$R_Q = \frac{1}{\tau_m} - \frac{1}{\tau_0} \tag{1}$$

- where τ_m is the measured value and τ_0 the radiative lifetime.

A quadratic dependence $R_Q \sim N^2$ corresponds to diffusion – limited processes whilst the linear $R_Q \sim N$ infers fast diffusion processes [18]. Hence a logarithmic plot of the quenching rate versus concentration should show a slope equal to two if the decay is diffusion –limited and equal to one in the case of fast diffusion.

Figure 5 shows a logarithmic plot of the quenching rate of the $^3H_4$ level as a function of the Tm^{3+} concentration. As can be observed in this concentration range the slope is 2.2 which indicate the presence of a dipole-dipole mechanism in the framework of a diffusion-limited regime. As we have mentioned before, for Tm^{3+} concentrations higher than 6 mol%, the emission from $^3H_4$ level is nearly totally quenched due to CR to $^3F_4$ level.

Non-exponential decay curves of $^3H_4$ emissions which are attributed to diffusion – limited regime when energy transfer between sensitizers and sensitizer to activator via dipole – dipole interaction occurs can be fitted by the Yokota – Tanimoto (Y-T) equation [19]:

$$\phi(t) = \phi(0) \cdot e^{-t/\tau_0} \cdot \exp\left[-\frac{4}{3} \cdot \pi^{3/2} \cdot N \cdot (C_{SA} \cdot t)^{1/2} \cdot \left(\frac{1+10.87x+15.5x^2}{1+8.743x}\right)^{3/4} \right] \tag{2}$$

where τ_0 is radiative lifetime, N is dopant concentration, $x = 0.5 \cdot (\frac{4\pi}{3})^{4/3} \cdot C_{SS} \cdot C_{SA}^{-1/3} \cdot N^{4/3} \cdot t^{2/3}$, C_{SA} and C_{SS} are ET microparameters for SA and SS interaction respectively. The following parameterization can be used: $A = \frac{4}{3}\pi^{3/2} \cdot N \cdot C_{SA}^{1/2}$, $B = 0.5 \cdot (\frac{4\pi}{3})^{4/3} \cdot C_{SS} \cdot C_{SA}^{-1/3} \cdot N^{4/3}$. Value of parameter B can be expressed also as $B = DC_{SA}^{-1/3}$ with D as a diffusion coefficient [20]. Example of the fit curve for the sample T1 in a semilogarithmic plot is shown in fig. 6. For Tm^{3+} doping levels higher than $6.84 \cdot 10^{20}$ cm^{-3}, the emission from $^3H_4$ level is practically quenched.

Obtained values of Y-T parameters are shown in Table 6.

This table also shows the values for the critical radius R_0. The critical distance R_0 taken as $R_0^6 = \tau_0 C_{SA}$ indicates that the energy transfer can occur among ions which are located within a given domain. A longer critical distance value means faster energy transfer.

Parameters A and B can be extended for the various concentration values by plotting them versus dopant concentration (Fig 7a, b).

From the slope of the parameter A, $C_{SA} = 2.15\ 10^{-50}$ m^6/s can be obtained which in turn is used together with the slope of the parameter B to give $C_{SS} = 1.16\ 10^{-50}$ m^6/s. These values are of the same order as those obtained from fits of the experimental decays from level $^3H_4$ to the Yokota - Tanimoto model. In this case $C_{SS} < C_{SA}$ so the probability of energy transfer to acceptor is higher than to sensitizer.

Another possibility to evaluate the effect of the energy transfer on the lifetimes of the $^3H_4$ level is to use rate equation formalism. By using this formalism and considering a low excitation density, Camargo et al. [21] obtained the following expression for the lifetimes of the $^3H_4$ level as a function of concentration:

$$\tau_{calc.} = \frac{\tau_0}{1 + W_{ET} \cdot N \cdot \tau_0} \quad (3)$$

where τ_0 is the radiative lifetime of $^3H_4$ level, W_{ET} the total energy transfer for dd interaction and N sensitizer ion concentration. In this study ET microparameters of dd interaction are obtained trough Yokota – Tanimoto fitting and not by Kushida model. Therefore is taken: $W_{ET}^{dd} = 28(C_{SA}^{dd})^{1/4}(C_{SS}^{dd})^{3/4}N$ [22]. W_{ET} should include contribution from dq and qq interaction which is in our case excluded. Values of calculated and measured lifetimes are shown on Fig. 8.

ET microparameters of Tm^{3+} in ZB(L)AN glasses for the $^3H_4$ level reported in literature [19] are: C_{SS} = 2.8 10^{-51} m^6/s, C_{SA} = 3 10^{-51} m^6/s. Values reported by Balda [20] where the host material was TeO_2-WO_3-PbO glass and Burshtein model applied are ~ 10^{-51} m^6/s. Values of 5.15 10^{-51} m^6/s obtained by Yokota–Tanimoto fit on the $^3H_4$ decay curve of Tm^{3+} in TeO_2–$CdCl_2$ glass is reported by [23]. C_{SA} parameter from this study obtained by Yakota–Tanimoto fitting for the sample T1 is of the same order of magnitude as in the literature whilst by parameter extension by fitting gives higher values. Both parameters, C_{SA} and C_{SS} showed good range of order by inserting them to ET constant and comparing obtained lifetime values with the experimental results.

3.5. Concentration quenching of the $^3F_4$ emission

Concerning the $^3F_4$ emission, the relative luminescence intensity increases while its lifetime decreases with concentration. Figure 9 shows the logarithmic plot of the experimental decays of the $^3F_4$ level for all samples. As can be seen the decays can be described by an exponential function to a good approximation for all concentrations and the lifetime decreases as concentration increases. Lifetime values and the corresponding quantum efficiency for the $^3F_4$ emission are reported in Table 5.

In this case, where the $^3F_4$ level is the first excited state, the quenching of luminescence when active ion concentration increases can not be due to cross-relaxation between various excited states and it has been mainly considered as due to diffusion towards unidentified impurities (such as OH or other impurities present in the starting materials). The problem can be separated into two cases: diffusion limited regime and fast diffusion. The first case is considered when the order of magnitude for transfer probability between sensitizers and sensitizer to activator are the same. As we have seen, in the case of the diffusion limited situation the quenching rate is proportional to the square of concentration. As it is shown in Fig. 5 a logarithmic plot of the quenching rate of level $^3F_4$ as a function of Tm^{3+} concentration gives a slope close to 2, which indicates that we are dealing with a diffusion limited regime. In such a case, and assuming a dipole-dipole interaction, the self quenching behavior can be described by the formula proposed by Auzel [24]:

$$\tau = \frac{\tau_0}{1 + \frac{9}{2 \cdot \pi}\left(\frac{N}{N_0}\right)^2} \tag{4}$$

where τ is measured lifetime at given concentration N, τ_0 is lifetime for low concentrations i.e. radiative lifetime, N_0 as the critical sensitizer concentrations is linked with critical distance between sensitizer and trap as $R_0 = \left(\frac{3}{4 \cdot \pi \cdot N_0}\right)^{1/3}$. By fitting of experimentally obtained lifetime values on the above formula (Fig. 10) the following characteristic parameters can be obtained: τ_0 = (3.29±0.07) ms, N_0 = (4.2±0.1) 10^{20} cm^{-3}, R^2= 0.997, $R_0(^3F_4)$ = 8.3 Å → C_{SA} = 9.8 10^{-53} m^6/s.

Experimental values are in very good agreement with the fit curve for the whole range of concentrations. ET parameter is lower than in the case of $^3H_4$ level by three orders of magnitude and the critical radius, shorter.

4. Conclusions

The present study concerns the investigation of various highly doped Tm^{3+} tellurite glasses in order to provide optimum dopant concentration for short cavity laser. Lifetime values of low doped sample have been measured and the obtained values of 3.09 and 0.347 ms for $^3F_4$ and $^3H_4$ level, respectively. The optimum emission intensity at 1.8 μm considering single ion was obtained for the concentration of 6.84 10^{20} cm^{-3} Tm^{3+} with 24% quantum efficiency. For such a high dopant concentration CR process strongly quenches emission from $^3H_4$ level. An analysis of the fluorescence decays of the $^3H_4 \rightarrow {}^3F_4$ emission as a function of concentration reveals that the electronic mechanism responsible for the ion-ion interaction is a dipole-dipole quenching process in the framework of a diffusion-limited regime. The self-quenching of the 1.8 μm emission can be attributed to limited diffusion within the active centers. This means that the probability for the diffusive steps between active centers is of the same order of magnitude than the one for quenching between impurities and centers. A critical sensitizer concentration for self quenching of 4.2 10^{20} cm^{-3} was obtained. This dopant concentration could be extended to the 6.84 10^{20} Tm^{3+} with a satisfactory QE in order to obtain short cavity fiber laser devices.

Acknowledgments

The authors wish to thank the Regione Piemonte Converging Technologies "Hipernano" research project. R. Balda and J. Fernández acknowledge financial support from the Spanish Ministerio de Ciencia e Innovacion under project MAT2009-14282-C02-02 and from the Basque Country Government (IT-331-07).

5. References

[1] Masayuki Yamane, Yoshiyuki Asahara, Glasses for Photonics, Cambridge University Press, ISBN-13: 9780521580533, p. 131., 2004.

[2] W.E.K. Gibbs, D.J. Booth, V.K. Bogdanov, Population dynamics of the $^3F_4$ and $^3H_4$ levels in highly-doped Tm^{3+}:ZB(L)AN glasses, Journal of Non-Crystalline Solids, 353, (2007).

[3] A. Godard, Infrared (2–12 μm) solid-state laser sources: a review C. R. Physique, 8, (2007).

[4] J. F. Digonnet, Rear –Earth doped fiber laser and amplifiers, sec. edition, Marcel Dekker, p. 627, (2001).

[5] Encyclopedia of Laser Physics and Technology, RP – Photonics, http://www.rp-photonics.com

[6] H. Gebavi, D. Milanese, G. Liao, Q. Chen, M. Ferraris, M. Ivanda, O. Gamulin, S. Taccheo, Spectroscopic investigation and optical characterization of novel highly thulium doped tellurite glasses, J. Non. Cryst. Solids, vol. 355, no 9, p.548 – 555, (2009).

[7] R. Rolli, M. Montagna, S. Chaussedent, A. Monteil, V.K. Tikhomirov, M. Ferrari, Erbium-doped tellurite glasses with high quantum efficiency and broadband stimulated emission cross section at 1.5 μm, Optical Materials 21, 743–748, (2003).

[8] B. M. Walsh, Norman P. Barnes, Donald J. Reichle, Shibin Jiang, Optical properties of Tm^{3+} ions in alkali germanate glass, J. of Non-Crystalline Solids 352, 5344–5352, (2006).

[9] Elizabeth R. Taylor, Li Na Ng, and Neil P. Sessions, Herbert Buerger, Spectroscopy of Tm^{3+}-doped tellurite glasses for 1470 nm fiber amplifier, J. Appl. Phys., vol. 92, no. 1, (2002).

[10] J. Alloys and Compounds 436 (2007) 216.

[11] Yong Gyu Choi , Doo Hee Cho, Kyong Hon Kim Influence of 4f absorption transitions of Dy^{3+} on the emission spectra of Tm^{3+}-doped tellurite glasses, J. Non-Crystalline Solids, 276, 1-7, (2000).

[12] Craig A. Evans, Zoran Ikonic, Billy Richards, Paul Harrison, Animesh Jha, Numerical Rate Equation Modeling of a ~ 2.1 μm Tm^{3+}/Ho^{3+} Co-Doped Tellurite Fiber Laser, J. Lightwave Tech., vol. 27, no. 19, (2009).

[13] D. F. de Sousa, R. Lebullenger, A. C. Hernandes, L. A. O. Nunes, Evidence of higher-order mechanisms than dipole-dipole interaction in Tm^{3+} - Tm^{3+} energy transfer in fluoroindogallate glasses, Phy. Rev. B, vol. 65, (2002).

[14] M. Ajroud, M. Haouari1, H. Ben Ouada, 1, H. Mâaref, A. Brenier, and B. Champagnon, Study of the spectroscopic properties and infrared-to-visible up-conversion fluorescence of Er^{3+}-doped germanate glasses, Phys. stat. sol., 202, no. 2, 316–329, (2005).

[15] J.R. Lakowicz, Principles of fluorescence spectroscopy, Kluwer Academic/Plenum Publishers, New York, (1999).

[16] B.M. Walsh, Review of Tm and Ho Materials; Spectroscopy and Lasers, Laser Physics, vol.19. no. 4., p. 855-866, (2009).

[17] Marvin J. Weber, Luminescence decay by energy migration and transfer; Observation of diffusion – limited relaxation, Phy. Review B, vol. 4, 9, (1971).

[18] F. Auzel, F. Bonfigli, S. Gagliari, G. Baldacchini, The interplay of self-trapping and self-quenching for resonant, transitions in solids; role of a cavity, J. of Lumin. 94–95, 293–297, (2001).

[19] W.E.K. Gibbs, D.J. Booth, V.K. Bogdanov, Population dynamics of the $^3F_4$ and $^3H_4$ levels in highly-doped Tm^{3+}:ZB(L)AN glasses, J. Non-Crystalline Solids, 353, 1–5, (2007).

[20] R. Balda, L.M. Lacha, J. Fernandez, M. A. Arriandiaga, J.M. Fernandez-Navarro, D. Munoz-Martin, Spectroscopic properties of the 1.4μm emission of Tm^{3+} ions in TeO_2-WO_3-PbO glasses, Opt. Express, vol.16, no.16, (2008).

[21] A.S.S. de Camargo, S.L. de Oliveira, D.F. de Sousa, L.A. O. Nunes, D.W.Hewak, Spectroscopic properties and energy transfer parameters of Tm^{3+} ions in gallium lanthanum sulfide glass, J. Phys. Condens. Matter 14 , 9495-9595, (2002).

[22] D. F. de Sousa, L. A. O. Nunes, Microscopic and macroscopic parameters of energy transfer between Tm^{3+} ions in fluoroindogallate glasses, Phy. Review B 66, 024207, (2002).

[23] A. Sennaroglu, A. Kurt, G. Ozen, Effect of cross relaxation on the 1470 and 1800 nm emissions in Tm^{3+}:TeO_2–$CdCl_2$ glass, J. Phys.: Condens. Matter 16, 2471–2478, (2004).

[24] F. Auzel, F. Bonfigli, S. Gagliari, G. Baldacchini, The interplay of self-trapping and self-quenching for resonant, transitions in solids; role of a cavity, J. of Lumin. 94–95, 293–297, (2001).

Tables

Table 1. Concentration and refractive indexes for Tm-doped 75T-20Z-5N glasses

Sample name	Tm^{3+} $x10^{20}(cm^{-3})$	n(633nm)	n(825nm)	n(1061nm)	n(1312nm)	n(1533nm)
T0	0	2.0514	2.0243	2.0091	2.0012	1.9962
T0.36	0.82	2.0488	2.0224	2.0077	1.9998	1.9950
T1	2.28	2.0454	2.0189	2.0046	1.9965	1.9918
T2.1	4.87	2.0412	2.0152	2.0007	1.9928	1.9880
T3	6.84	2.0396	2.0136	1.9994	1.9917	1.9867
T4	9.06	2.0356	2.0097	1.9954	1.9983	1.9833
T5	11.3	2.0306	2.0053	1.9913	1.9839	1.9792
T6	13.5	2.0268	2.0021	1.9879	1.9805	1.9761
T7	15.7	2.0239	1.9993	1.9853	1.9780	1.9733
T10	22.1	2.0116	1.9878	1.9746	1.9672	1.9629

* T0 signs host composition

Table 2. J-O parameters comparison with literature.

Reference	Ω_2	Ω_4	Ω_6
[8]*	3.38	2.17	1.17
[10]*	4.64	1.61	1.26
[11]**	5.106	1.174	1.082
This study *	4.4	1.97	1.22

* host composition: $75TeO_2$-20ZnO-$5Na_2O$

** host composition: $80TeO_2$-10ZnO-$10Na_2O$

*** Ω [10^{-20} cm^2]

Table 3. Transition rates, radiative lifetimes, and branching ratios

Transition	$\bar{\lambda}$ (nm)	$A_{J'J}$ (s^{-1})	τ_0 (ms)	β
$^1G_4 \rightarrow {}^3H_6$	470	2803.82	0.19	0.5445
$^1G_4 \rightarrow {}^3F_4$	646	354.99		0.0689
$^1G_4 \rightarrow {}^3H_5$	763	1446.24		0.2808
$^1G_4 \rightarrow {}^3H_4$	1177	442.71		0.0859
$^1G_4 \rightarrow {}^3F_3$	1494	102.07		0.0198
$^3F_3 \rightarrow {}^3H_6$	686	4396.45	0.2	0.8381
$^3F_3 \rightarrow {}^3F_4$	1138	118.43		0.0226
$^3F_3 \rightarrow {}^3H_5$	1558	724.36		0.1381
$^3F_3 \rightarrow {}^3H_4$	5552	6.36		0.0012
$^3H_4 \rightarrow {}^3H_6$	784	2685.6	0.36	0.9035
$^3H_4 \rightarrow {}^3F_4$	1432	226.71		0.0762
$^3H_4 \rightarrow {}^3H_5$	2166	60.25		0.02
$^3H_5 \rightarrow {}^3H_6$	1225	$459.6_{ED}+113.3_{MD}$	1.71	0.9793
$^3H_5 \rightarrow {}^3F_4$	4226	12.12		0.0207
$^3F_4 \rightarrow {}^3H_6$	1725	488.13	2.1	1

Table 4. Lifetime values comparison

Transition	τ_0 (ms) This study	τ_0 (ms) exp. values	τ_0 (ms) [8]	τ_0 (ms) [9]	τ_0 (ms) [10]
$^3F_4 \rightarrow {}^3H_6$	2.1	3.09	3	2.13	2.1
$^3H_5 \rightarrow {}^3H_6$	1.71	NA	NA	1.88	1.63
$^3H_4 \rightarrow {}^3H_6$	0.36	0.347	0.35	0.37	0.34
$^3F_3 \rightarrow {}^3H_6$	0.2	NA	NA	NA	0.24
$^1G_4 \rightarrow {}^3H_6$	0.19	NA	NA	NA	0.19

Table 5. Lifetime values of $^3H_4$ and $^3F_4$ level with corresponding quantum efficiency

Sample name	Tm^{3+} $x10^{20}(cm^{-3})$	$^3H_4$ (μs)	$\eta(^3H_4)$ %	$^3F_4$ (ms)	$\eta(^3F_4)$ %
T0.36	0.82	347	100	3.09	100
T1	2.28	147	42.4	2.42	78.3
T2.1	4.87	32	9.2	1.06	34.3
T3	6.84	18	5.2	0.74	23.9
T4	9.06	7	2	0.42	13.6
T5	11.3	7	2	0.32	10.4
T6	13.5	5	1.4	0.14	4.5
T7	15.7	4	1.2	0.14	4.5
T10	22.1	4	1.2	0.04	1.3

Table 6. Obtained values of the Yakota – Tanimoto fitting parameters

$^3H_4$ level	A ($s^{-1/2}$)	B ($s^{-2/3}$)	R^2 (%)	C_{SA} $10^{-50}(m^6/s)$	D $10^{-14}(m^2/s)$	R_0 (Å)
T1	119±1	92±3	99.65	0.49	0.16	10.9
T2.1	400±4	491±14	99.27	1.23	1.13	12.7
T3	616±7	744±18	98.48	1.47	1.82	13.1

*R^2 is the square of the correlation coefficient

Figures

Fig.1. Absorption cross section of Tm^{3+} doped TZN glass

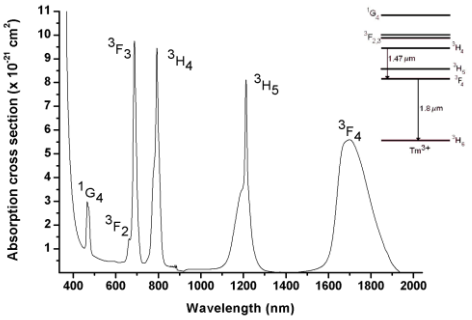

Fig. 2. Emission spectra of thulium $^3H_4$ and $^3F_4$ levels. All the spectra are normalized on the area under $^3H_4$ peak.

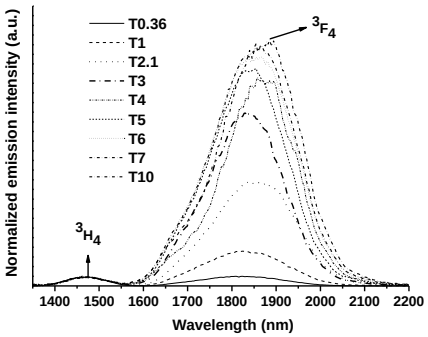

Fig. 3a) Emission ratio presents the ratio between area under $^3F_4 \rightarrow {}^3H_6$ and $^3H_4 \rightarrow {}^3F_4$ emission bands. The line is a guide to the eye.

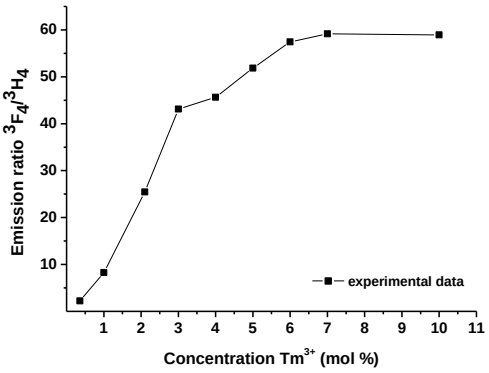

Fig. 3b) Ratio between the areas under the $^3F_4 \rightarrow {}^3H_6$ and $^3H_4 \rightarrow {}^3F_4$ emission bands normalized to the number of ions.

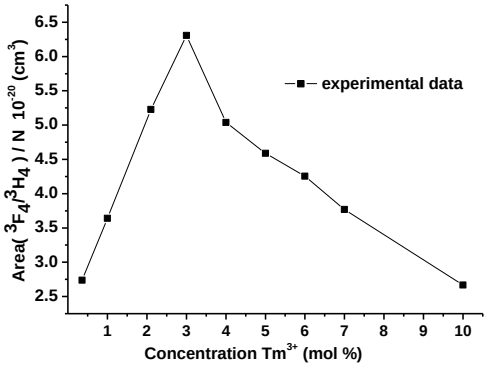

Fig. 4. Lifetime decay curves of $^3H_4$ level. Exponential decay is only in the case of sample T0.36

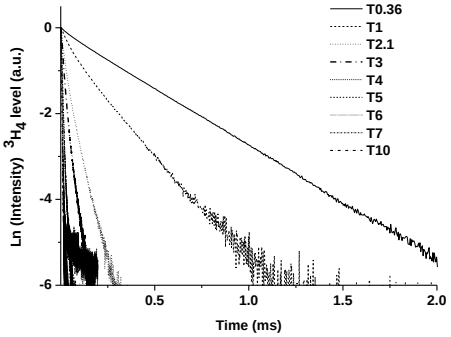

Fig. 5. Logarithmic dependence of quenching rate and dopant concentration. Curve slopes for both $^3H_4 \rightarrow {}^3H_6$, $^3F_4 \rightarrow {}^3H_6$ transitions are around 2.

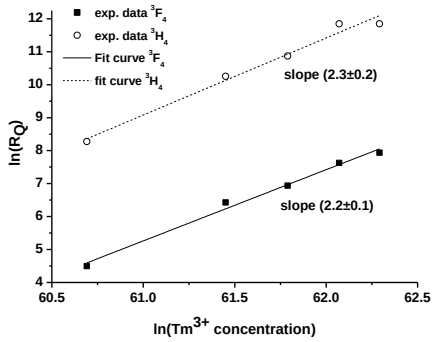

Fig. 6. Yokota-Tanimoto fit for $^3H_4$ level of the sample T1.

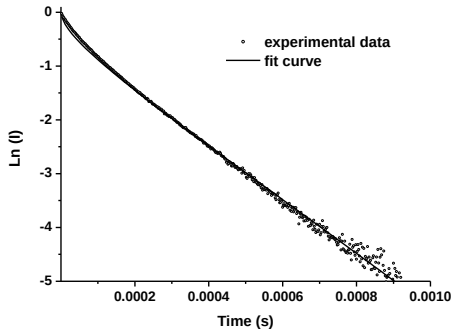

Fig. 7a) Yokota – Tanimoto fit parameter A as a function of concentration: A = (1.089±0.003) 10^{-24}N

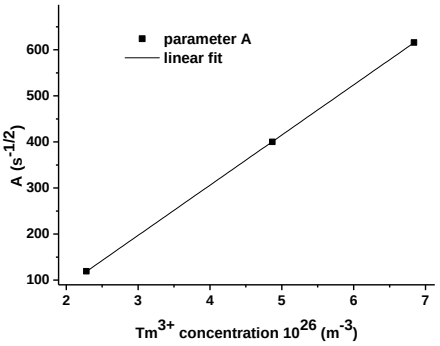

Fig. 7b) Yokota – Tanimoto fit parameter B as a function of $N^{4/3}$ concentration: B = (1.4±0.1)10^{-33} $N^{4/3}$

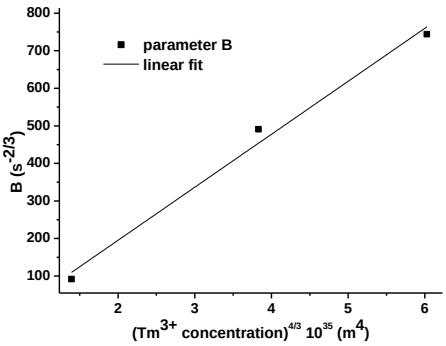

Fig. 8. Calculated and measured lifetime values of the $^3H_4$ level. Deviation from experimental values is smaller for higher dopant concentrations.

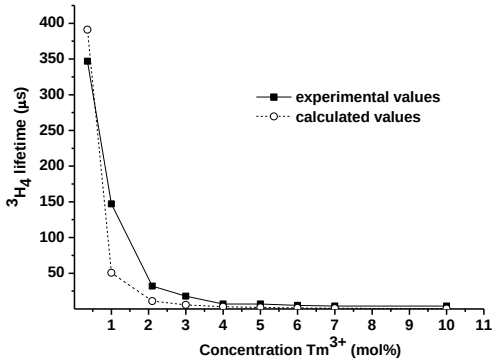

Fig. 9. Decay curves of $^3F_4$ emissions. Sample T1 shows non-linear behavior.

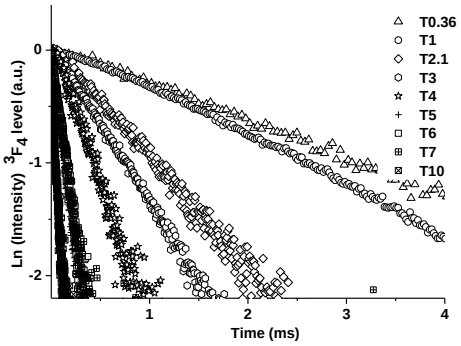

Fig. 10. Experimental data of $^3F_4$ level fitted on theoretical curve. Values of 8.3 Å for critical distance and corresponding N_0 = (4.2±0.2) 10^{20} cm^{-3} and ET microparameter 9.8 10^{-53} m^6/s are obtained.